Magnetic flaring in the pre-main sequence Sun and implications for the early solar system

Eric D. Feigelson, Gordon P. Garmire

Department of Astronomy & Astrophysics, Pennsylvania State University, University Park PA 16802

`edf@astro.psu.edu`

and

Steven H. Pravdo

Jet Propulsion Laboratory, MS 306-438, 4800 Oak Grove Drive, Pasadena CA 91109

ABSTRACT

To address the role of energetic processes in the solar nebula, we provide a detailed characterization of magnetic flaring in stellar analogs of the pre-main sequence Sun based on two 0.5-day observations of analogs of the young Sun in the Orion Nebula Cluster obtained with the *Chandra X-ray Observatory*. The sample consists of 43 stars with masses 0.7-1.4 $M_\odot$ and ages < 0.3 to $\simeq 10$ My. We find the X-ray luminosities measured in the $0.5 - 8$ keV band are strongly elevated over main sequence levels with average $< \log L_x >= 30.3$ erg s^{-1} and $< \log L_x/L_\star >= -3.9$. The X-ray emission is strongly variable within our exposures in nearly all solar analogs; about 30 flares with $29.0 < \log L_x(peak) < 31.5$ erg s^{-1} on timescales from 0.5 to > 12 hours are seen during the Chandra observations. Analogs of the ≤ 1 My old pre-main sequence Sun exhibited X-ray flares that are $10^{1.5}$ times more powerful and $10^{2.5}$ times more frequent than the most powerful flares seen on the contemporary Sun.

Radio observations indicate that acceleration of particles to relativistic energies is efficient in young stellar flares. Extrapolating the solar relationship between X-ray luminosity and proton fluence, we infer that the young Sun exhibited a 10^5-fold enhancement in energetic protons compared to contemporary levels. Unless the flare geometries are unfavorable, this inferred proton flux on

the disk is sufficient to produce the observed meteoritic abundances of several important short-lived radioactive isotopes. Our study thus strengthens the astronomical foundation for local proton spallation models of isotopic anomalies in carbonaceous chondritic meteorites. The radiation, particles and shocks produced by the magnetic reconnection flares seen with *Chandra* may also have flash melted meteoritic chondrules and produced excess ^{21}Ne seen in meteoritic grains.

Subject headings: meteors, meteoroids; solar system: formation; Sun: activity; stars: pre-main-sequence; X-rays: stars

1. Introduction

A large body of meteoritic evidence indicates that violent high-energy processes occurred in or near the solar nebula during the formation of the solar system. The prevalence of chondrules requires sudden heating of solid material to $T \simeq 2000$ K, likely produced by shocks, lightning or radiation in the solar nebula (see reviews in Hewins, Jones, & Scott 1996; Jones et al. 2000). Anomalous abundances of elemental isotopes are seen in chondrules and inclusions of the most pristine carbonaceous chondrites (see review by Goswami & Vanhala 2000). Most puzzling are the high abundances of daughter products of short-lived nuclides like ^{41}Ca, ^{26}Al and ^{53}Mn. These nuclides are often attributed to the injection of freshly produced nuclear products into the nebula from stellar sources: a supernova remnant or winds from an asymptotic giant branch (AGB) or Wolf-Rayet star (Cameron & Truran 1977; Wasserburg et al. 1994; Arnould, Paulus, & Meynet 1997).

An alternative explanation involves the production of unusual nuclear species within the nebula by spallation reactions from energetic (MeV) protons and ions originating in magnetic reconnection flares. Energetic particles are currently produced in the solar system by flares above the Sun's surface, but with fluences far below those required by local irradiation models of short-lived meteoritic nuclides. In early calculations (e.g. Hoyle, Fowler & Greenstein 1962; Clayton, Dwek, & Woosley 1977; Lee 1978), local irradiation models had difficulty producing nuclides in the observed abundances. Various problems have been addressed in recent studies that, for example, investigate spallation principally in the circumstellar disk corona, consider production of meteoritic isotopes such as ^{138}La and ^{10}Be in addition to well-known isotopes such as ^{26}Al and ^{41}Ca, and examine the effects of ^{3}He-rich flares and self-shielding by chondrule rim material (Clayton & Jin 1995; Lee et al. 1998; Gounelle et al. 2001; Goswami, Marhas, & Sahijpal 2001). Spallogenic isotope production by cosmic rays pervading star forming regions has also been considered (Clayton 1994), but an early report

of $\gamma-$ray lines in the Orion region supporting this model has been withdrawn (Bloemen et al. 1999).

Some meteoritic abundance anomalies are more plausibly explained by local spallation of solar nebular solids than by injection of stellar nucleosynthetic material. ^{21}Ne is readily produced by proton spallation reactions on common rock-forming elements like Mg and Si, and is present with high abundance in certain grains of carbonaceous chondrites (e.g. Caffee et al. 1987; Rao et al. 1997; Caffee & Nishiizumi 2001, see review by Woolum & Hohenberg 1993). A spallation origin is supported by high particle track densities in the crystalline grain. This combination of evidence implies that the grains were subject to high proton fluences while free-floating in the nebula prior to meteoritic compaction. Similarly, the spallogenic product ^{10}Be has recently been reported in the Allende meteorites consistent with a local irradiation model (McKeegan et al. 2000), although production in an anisotropic jet during a supernova explosion is also possible (Cameron 2001). The recent discovery of ^{36}Ar and other noble gases in silicate chondrites also points to an enhanced solar wind prior to chondrule melting (Okazaki et al. 2001).

In addition to spallation, magnetic reconnection flares produce sudden increases in the photon flux and (unobserved but plausible by analogies with solar flares) shocks within the solar nebula environment. These may be responsible for the flash melting of chondrules (Levy & Araki 1989; Taylor 1992; Shu et al. 1997, 2001). Although local irradiation and shock models often call for enhanced magnetic activity in the early Sun, the size, location and geometry of the flaring magnetic fields is uncertain. Field lines may be rooted in the proto-solar surface as in the contemporary Sun (e.g. Feigelson, Giampapa, & Vrba 1991), may link the proto-Sun to the nebula at the corotation radius at ~ 10 R$_\odot$ (e.g. Shu et al. 1997; Montmerle et al. 2000; Birk et al. 2000), may erupt from an turbulent magnetohydro-dynamical (MHD) nebula (e.g. Levy & Araki 1989; Romanova et al. 1998; Priest & Forbes 2000, 455ff), or may be produced by interactions between the solar wind and the nebula at planetary distances (Cameron 1995). The magnetic geometry issue will be discussed here in §6.3.

Astronomical studies of young solar analogs can provide valuable insights into these issues. For example, although injection freshly synthesized material from a passing AGB star is an attractive explanation for the origin of several short-lived nuclides (Busso, Gallino, & Wasserburg 1999), the chances are very small that an AGB star passes sufficiently close to any given molecular cloud for this mechanism to operate (Kastner & Myers 1994). Triggering by supernova shocks does occur, but may affect only a fraction of star forming sites (Adams & Laughlin 2001).

On the other hand, a large body of astronomical studies of young solar-type stars sup-

ports the idea that high levels of magnetic flaring are present in virtually all stars through all stages of pre-main sequence evolution (see review by Feigelson & Montmerle 1999). This provides an empirical basis to local spallation models for meteoritic isotopic anomalies. X-ray emission from pre-main sequence low-mass stars is enhanced $10^1 - 10^4$ times above levels seen in the Sun today, exhibiting high plasma temperatures ($T \sim 10^7 - 10^8$ K) and rapid high-amplitude variability indicative of violent magnetic reconnection events. Nonthermal radio continuum flaring has been detected in a smaller fraction of young stars (see review by André 1996). This is demonstrably gyrosynchrotron emission from MeV electrons spiraling in magnetic fields, direct evidence for particle acceleration to MeV energies in pre-main sequence systems. Extensive evidence (photometric starspots, Doppler imaging, Zeeman line splitting, chromospheric indicators, etc.) has also accrued indicating that T Tauri stars have highly magnetized stellar surfaces. The link between X-ray flaring in T Tauri stars and meteoritic issues has been discussed by Feigelson (1982), Feigelson et al. (1991), Shu et al. (1997), Feigelson & Montmerle (1999) and Priest & Forbes (2000, 455ff).

Past studies of magnetic activity in analogs of the early Sun have suffered practical limitations. Some individual $\simeq 1$ M$_\odot$ young stars have been studied in detail, such as V410 Tau or EK Dra (e.g. Herbst 1989; Strassmeier & Rice 1998), but it is unclear whether these represent the average case or outliers with unusually rapid rotation and magnetic activity. X-ray emission was surveyed in young stellar clusters in nearby star forming clouds with the *Einstein* and *ROSAT* orbiting X-ray telescopes (reviewed in Feigelson & Montmerle 1999). But the resulting samples typically have < 100 stars across the initial mass function with only a handful of solar analogs. Richer young stellar clusters in more distant giant molecular clouds were examined with *ROSAT*, but its optics could not resolve the crowded fields and only the strongest flares could be detected.

We report here an observational study of the young solar analogs in the richest unobscured young star cluster in the nearest giant molecular cloud: the Orion Nebula Cluster, whose OB members ionize the Orion Nebula (Messier 42). The study is conducted with the recently-launched *Chandra X-ray Observatory*. *Chandra*'s superb mirrors provide arcsecond spatial resolution, and the Advanced CCD Imaging Spectrometer (ACIS) detector at its focal plane provides high quantum efficiency with very low background noise and independent spectroscopy of each star. The satellite has a high-ellipticity orbit that permits continuous observation over many hours.

Our principal goal here is to establish unbiased quantitative measures of magnetic activity in young solar-like stars which can serve as empirical input into local irradiation models for meteoritic isotopic anomalies and shock models for chondrules formation.

2. Observations and data reduction

The Orion Nebula Cluster (ONC) is the richest young star cluster within 500 pc with $\simeq 2000$ members concentrated in a 1 pc (8') radius sphere (O'dell 2001). The full initial mass function from a 45 $M_\odot$ O star to dozens of substellar brown dwarfs is present. Most of the stars are optically visible (i.e. are not deeply embedded in the Orion molecular cloud and are not heavily absorbed) with $V < 20$ magnitudes. These stars have well-characterized photometry and spectroscopy from which bolometric luminosities and spectral types are measured on the Hertzsprung-Russell diagram (Hillenbrand 1997). Their locations on the HR diagram are then compared to theoretical stellar interior models (D'Antona & Mazzitelli 1997) so that stellar ages and masses can be inferred. While most of the stars have ages ≤ 1 My, some have lower luminosities implying ages of $5 - 20$ My. An additional population of deeply embedded stars lies behind the ONC around the OMC 1 cloud cores, but these will not concern us here.

The ONC was observed with the ACIS-I imaging array on board *Chandra* twice during the inaugural year of the satellite, on 12 Oct 1999 and 1 Apr 2000, for $\simeq 12$ hours on each occasion. The satellite is described by Weisskopf et al. (1996) and details of the ACIS instrument are available at http://www.astro.psu.edu/xray/acis. Garmire et al. (2000) gives a report of the first observation, and a full description of the data reduction and sources found in both observations is given by Feigelson et al. (2001, hereafter F01). We summarize these procedures briefly here.

The satellite telemetry data were corrected for charge transfer inefficiency, cleaned of cosmic ray afterglows, hot columns, undesirable grades and energies. The two observations were merged, and astrometrically aligned to the Hipparcos frame using 2MASS sources to $\pm 0.1''$ accuracy. Source detection based on a wavelet transform algorithm located 1075 sources with a sensitivity limit of 9 counts ($L_x \simeq 1 \times 10^{28}$ erg s^{-1} for a typical unabsorbed spectrum) near the field center. Source photons were extracted from the 95% or 99% encircled energy circle except where crowding is present. Background is negligible in most cases and is not subtracted here. Effective exposure times include effects of telemetry dropouts, telescope vignetting, and point spread function wings. The total exposure time near the field center is 83 ks. Least-squares spectral fitting to the pulse height distributions were performed assuming a Raymond-Smith plasma with soft-energy absorption, all assuming cosmic elemental abundances. A two-temperature plasma model was adopted when needed for satisfactory spectral fits. Most of the observed emission is attributable to optically thin plasma emission with $T \simeq 10 - 30$ MK (MK = 10^6 °K), though some plasma with $T \geq 100$ MK can be present. The ACIS-I detector is insensitive to plasma cooler than $T \leq 3$ MK.

The merged ACIS-I field is shown in Figure 1 in the $0.5 - 8$ keV total energy band. This is

the richest field of X-ray sources ever obtained in the history of X-ray astronomy. 92% of the X-ray sources are unambiguously identified with optical/infrared ONC cluster members with angular offsets $< 1''$ in the inner $10'$ where the telescope point spread function is optimum. For the X-ray and optically bright stars under discussion here, there is little doubt that the stellar identifications are correct with one caveat: most of the stars are probably binary or multiple systems at angular scales smaller than *Chandra*'s arcsecond resolution (Mathieu 1994). In the case of visual binaries (those with 'a' or 'b' in their names in Table 1), we associate the X-ray source with the brighter member of the system (see footnotes of Table 2 in F01 for individual cases).

3. Selection and X-ray properties of ONC solar analogs

In this study of analogs of the pre-main sequence Sun, we select for study all well-characterized ONC stars with $V < 20$ (Hillenbrand 1997) with inferred masses in the range $0.7 \leq M < 1.4$ M$_\odot$. Mass is chosen as the critical discriminant because it is the strongest predictor of X-ray emission in pre-main sequence stars (Feigelson et al. 2002). These 43 stars are listed in Table 1 and marked in Figure 1. All but two, shown as squares in Figure 1, are associated with ACIS X-ray sources. This is a unique ensemble of pre-main sequence with masses very close to 1 M$_\odot$ that have uniform distances, excellent optical/infrared characterization, and nearly complete X-ray detections from a survey with nearly uniform sensitivity.

The sample is complete for unobscured portions of the ONC, and includes a few of moderately absorbed stars. It suffers one selection bias: roughly $10 - 20$ ONC stars seen from JHK infrared images lie in our mass range but are sufficiently deeply embedded that their visual magnitudes $V > 20$ (Hillenbrand & Carpenter 2000). Unless some surprising link between large-scale gaseous environment and X-ray emission is present, the omission of these embedded stars from the sample studied here should have no effect on our results other than the removal of $\simeq 20$ random objects from the full cluster sample of solar-mass stars. We therefore consider the stars listed in Table 1 to be an unbiased sample of solar-mass pre-main sequence stars.

Table 1 lists the sample stars with relevant optical/infrared and X-ray properties. Most entries are extracted from Tables 2 and 3 of F01. Columns $1-2$ give the ACIS source number from F01 and its IAU designation. Column 3 gives the stellar counterpart from Jones & Walker (1988), and columns $4-6$ give the luminosity, visual absorption and estimated age from Hillenbrand (1997). Note that we have truncated ages below $\log t < 5.5$ yr due to the uncertainties in theoretical modeling of the initial conditions and effects of accretion (e.g. Wuchterl & Klessen 2001). Column 7 summarizes the evidence concerning a circumstellar

disk: a + symbol indicates a near-infrared photometric excess $\Delta(I - K) > 0.3$ and/or association with a Herbig-Haro outflow, far-infrared source or imaged proplyd; a − symbol indicates $\Delta(I - K) < 0.3$ and no association of these types; and ... indicates insufficient information for classification. Column 8 gives the extracted ACIS counts in the $0.5 - 8$ keV band which are used to evaluate the X-ray properties. For the two undetected stars, upper limits to the extracted counts and X-ray luminosities were obtained following the procedure in §2.11 of F01. Columns $9 - 10$ give the count rates in the first and second ACIS exposures respectively. Column 11 gives the variability class defined in F01: Constant (Const), Long-Term Variable (LT Var) indicating significantly different count rates between the two exposures, Possible flare (Pos fl) and Flare indicating variability within one or both exposures. Columns $11 - 13$ give fitted spectral parameters: interstellar column density along the line of sight in H atoms cm^{-2}, plasma energy in keV (with two energies listed if a one-temperature model provided a poor fit to the spectrum), and an indicator that Spectral Features (S.F.) are present, possibly due to non-solar elemental abundances in the heated plasma.

Column 14 gives the X-ray luminosity $\log L_x$ in the total band derived by integrating the spectral model over the $0.5 - 8$ keV band and multiplying by $4\pi d^2$ with $d = 450$ pc. This is called L_t in F01 and is corrected for differences in source spectrum, off-axis point spread function and telescope vignetting losses but is not corrected for line-of-sight absorption. F01 also give soft band, hard band and absorption-corrected total band luminosities for each source. These values typically lie within ± 0.4 of $\log L_x$ and show the same behavior in scatter plots such as Figure 2. The $\log L_x$ values are averaged over both $\simeq 12$-hour ACIS exposures which, as seen in Figure 3, masks substantial variability of the sources. Considerable scatter in $\log L_x$ values is thus expected due to the limited temporal coverage of each star's flaring behavior, which is unavoidable in any study of high-amplitude stellar flaring.

4. X-ray evolution and flaring in ONC solar analogs

We first evaluate the time-averaged X-ray luminosities of ONC solar analogs to provide an overview of the level and longevity of enhanced magnetic activity during the pre-main sequence phase. Then the short-term variations are examined to quantify the intensity and frequency of magnetic reconnection flares.

4.1. Long-term evolution of pre-main sequence X-rays

The distribution of X-ray emission for solar-mass ONC stars as a function of disks and stellar age is shown in Figure 2. The mean[1] X-ray luminosity is $< \log L_x > = 30.1 \pm 0.5$ erg s^{-1} for the full sample and 30.3 ± 0.5 erg s^{-1} for the stars ≤ 1 My in age.

But Figure 2a suggests that the X-ray luminosity decreases as the star descends the Hayashi pre-main sequence tracks. An anticorrelation between L_x and age is present at a significance level of $P \simeq 0.003$, as evaluated by the generalized Spearman's ρ and Kendall's τ nonparametric tests for correlation[1]. A linear regression fit[2], shown as the dashed line, gives

$$\log L_x = 30.2(\pm 0.8) \ - \ 1.1(\pm 0.1) \log(t/10^6 \text{ yr}) \text{ erg s}^{-1}.$$

This finding suggests that magnetic activity decreases as the star ages from $\log t \simeq 5$ to 7 yr, but the correlation is based on only a few stars. This result was absent in early *Einstein Observatory* results (Walter & Barry 1991) and was tentatively reported in one *ROSAT* T Tauri sample (Feigelson et al. 1993), while another *ROSAT* study showed a rise in L_x up to $\log t \simeq 6.5$ yr followed by a decline (Neuhäuser et al. 1995).

We note from Figure 2a that the presence or absence of a circumstellar disk (filled or open circles) has no discernable effect on the level of X-ray emission. This result has been found in many X-ray studies of pre-main sequence stars (Feigelson & Montmerle 1999, F01), though diskless stars were found to be brighter in X-rays than classical T Tauri stars in a *ROSAT* study of the Taurus-Auriga clouds (Stelzer & Neuhäuser 2001).

Figure 2b shows the evolution of the ratio $\log L_x/L_\star$, which is very closely related to the X-ray surface flux $\log L_x/(4\pi R_\star^2)$. Here the mean value is $\log L_x/L_\star = -3.9 \pm 0.5$ (1σ) for the whole sample and there is no statistically significant age dependence ($P \simeq 0.3$). However, as noted by Garmire et al. (2000) in a preliminary analysis of this diagram, the magnetic

---

[1]The mean, population standard deviation, and tests for correlation are evaluated using survival analysis techniques which take into account the two nondetections (left censored data points). See Chapter 10 of Babu & Feigelson (1996) for methodological details and code ASURV at http://www.astro.psu.edu/statcodes for implementation.

[2]Here we use the ordinary least squares (OLS) bisector line which is the most reliable of OLS lines that treats the two variables symmetrically. Regression coefficient errors (1σ) are estimated both analytically and with bootstrap simulation. Upper limits are considered to be detections for this calculation. See Chapter 7.2 of Babu & Feigelson (1996) for methodological details and code SLOPES at http://www.astro.psu.edu/statcodes for implementation.

activity of older stars with $\log t > 6.0$ yr has a higher dispersion (± 0.8) than younger stars with $\log t \leq 6.0$ yr (± 0.4). The causes of this are unknown: neither the presence of a disk nor surface rotation accounts for this effect (Feigelson et al. 2002). Perhaps stars follow two tracks as they age, one group with roughly constant $\log L_x$ and rising $\log L_x/L_\star$ and another group with declining $\log L_x$ and roughly constant $\log L_x/L_\star$. In this hypothetical case, we could not ascertain whether or not the early Sun participated in the general decline of $\log L_x$ as it aged. Note that a plot of the mean $log L_x/L_\star$ and $\log t$ for all (mostly sub-solar mass) stars in several young stellar clusters based on $ROSAT$ data shows a factor of ~ 10 rise in $\log L_x/L_\star$ with age from $5 < \log t < 8$ (Kastner et al. 1997), suggesting that only some stars participate in the falling $\log L_x$ we find in Figure 2a. For the purposes of this study, we conclude only that X-ray emission in solar analogs is typically $\log L_x \simeq 30.0 - 30.5$ erg s^{-1} during the first 1-2 Myr.

4.2. Short-term temporal behavior of pre-main sequence X-rays

The Variability Class listed in Table 1 is a qualitative indicator of the degree and nature of the variations. Twenty-eight of the 41 detected stars (68%) of the sources show intraday variability (classes 'Flare' and 'Possible flare'). Of the remaining 13 sources (classes 'Constant' and 'Long-Term Variable', three show high-amplitude (factor > 3) differences between the two observations suggesting that a long-duration flare is present during the high flux observation. Most of the remaining sources are weak with reduced sensitivity to rapid flares. We thus find that while 2/3 of the sources directly show variations on timescales of hours, the true fraction may be substantially higher. It is difficult to establish this fraction quantitatively due to the wide range of source count rates.

Figure 3 shows the X-ray lightcurves for the 28 stars exhibiting intraday variability and for two stars (JW 553a and JW 907) exhibiting high-amplitude long-term variability. The diversity of temporal behaviors is evident from these 30 lightcurves. Some show fast high-amplitude flares with relatively brief durations of $1 - 4$ hours superposed on a 'quiescent' level (e.g. JW 454, 698 and 810), others show slow high-amplitude changes on timescales ≥ 12 hours likely to be long-duration flares (e.g. JW 328, 504b, 567, 596, 738 and 826). A few cases show two events during the same 12-hour interval (e.g. JW 457, 463, 769, 826). Some of the less dramatics variations, as well as those of stars not shown, may be attributed to rotational modulation of static coronal structures.

While one cannot reliably distinguish individual flares from quiescent levels in all sources, we estimate from Figure 3 that 30 flares with $29.0 \leq \log L_x(peak) \leq 31.5$ erg s^{-1} were present in the ONC solar analogs during our observations. Their power is weighted towards the more

rather than less luminous flares: 20 of these 30 events have $\log L_x(peak) \geq 30$ erg s^{-1}. Total energies in the X-ray band, $E_x = L_x t_f$ where t_f is the duration of the flares, range from 10^{32} to $> 10^{36}$ erg. Flaring is present in both older and younger pre-main sequence stars, those with and without circumstellar disks, and those with slow as well as rapid surface rotation. It is a ubiquitous phenomenon.

5.   ONC flares, solar flares and inferred proton fluences

The results from our Chandra ACIS observations of the ONC solar analogs most salient to the early Sun and solar nebula irradiation issues are the average luminosity, peak flare luminosities, and flare frequcies in comparison to levels seen on the Sun today.

We find that all solar-mass stars with ages ≤ 1 My, averaged over both temporal variations and stars with ages ≤ 1 My, show an average X-ray luminosity of $< \log L_x > = 30.3$ erg s^{-1} in the $0.5 - 8$ keV band. For comparison, in the same band the contemporary Sun emits typically $\log L_x \simeq 25.3$ erg s^{-1} with $T \simeq 1$ MK during its quiet phase, $\log L_x \simeq 27.0$ erg s^{-1} during maximum phase with $T \simeq 2 - 5$ MK, and around $\log L_x \simeq 28.0$ erg s^{-1} with $T \simeq 2 - 20$ MK during a powerful (2 Nov 1992) flare (Peres et al. 2000). The ONC solar analogs thus collectively show a factor of $\sim 10^4$ elevation in X-ray emission over the Sun averaged over the solar cycle, and $10^{2.5}$ elevation over the most luminous solar flares.

The prevalence of rapid X-ray variations and high plasma temperatures of $10 \leq T \leq 100$ MK indicate that pre-main sequence X-rays generally arise from flare rather than coronal phenomena, even when individual flare events are not clearly seen in the lightcurves[3]. For comparison, the most X-ray luminous flares of recent solar cycles had $\log L_x(peak) \simeq 28.5 \pm 0.5$ erg s^{-1} in the *Chandra* spectral band (see Appendix). Taking 10^{30} erg s^{-1} for the typical flare in our ONC sample, we find that ONC solar analogs exhibits flares $10^{1.5}$ times more X-ray luminous than these extreme solar events. The ONC flares are roughly 10^4 times more powerful than solar flares which occur with a daily frequency.

Our ONC dataset is collectively equivalent to 86 0.5-day observations of a single solar-mass pre-main sequence star spread over a long period of time. The observed ONC flare frequency is thus about 30 flares over 43 days or 1 flare every 1.4 days or 1×10^5 s. The maximal solar flares with $\log L_x(peak) \simeq 28.5$ erg s^{-1} occur roughly once every year or

---

[3]Most of the observed X-ray emission in ONC stars is also too hot to arise from accretion onto the stellar surface from the disk or environs (Lamzin 1999). See, however, Kastner et al. (2001) for a soft-spectrum T Tauri star where accretion may dominate the X-ray spectrum.

3×10^7 (Sammis, Tang, & Zirin 2000, see Appendix). The ONC flares we detect are thus occur roughly $10^{2.5}$ times frequently than the most powerful solar flares.

We can now estimate the time-averaged enhancement of X-ray flare luminosity of ONC solar analogs compared to the strongest contemporary solar long duration events: $10^{1.5}$ elevation in peak luminosity times $10^{2.5}$ more frequent occurrence gives a 10^4 enhancement in total flare X-ray emission. This is similar to the 10^4 factors we find comparing the ONC stars with the time-averaged X-ray luminosity and daily solar flares.

For application to computations of nuclear spallation reactions, we must consider that solar proton fluences scale non-linearly with solar X-ray luminosity in the sense that most of the protons are produced by the most powerful flares. This is usually expressed in terms of the frequency distribution of events as a function of energy E: the distribution of proton events, $dN/dE \propto E^{-1.15}$, is significantly flatter than the distribution of X-ray events, $dN/dE \propto E^{-1.6} - E^{-1.8}$ (Hudson 1991; Crosby, Aschwanden, & Dennis 1993). If this difference extends over the 10^2 extrapolation in luminosity between solar and ONC flares, one infers an additional 10^1 increase in proton fluences in the early Sun from the observed giant flares[4]. We note that there is no astrophysical basis for this extrapolation; it is possible that proton fluence saturates at some lower level, as appears to occur in the contemporary Sun (Reedy 1996, see Appendix). However, the existence of efficient acceleration of relativistic particles by pre-main sequence flares is observationally established by their radio gyrosynchrotron emission (§6.2).

The enhancement in proton fluences of < 1 My ONC solar analogs is thus inferred to be about 10^5 above that produced by the most powerful flares from the Sun today: $10^{1.5}$ from the increased X-ray luminosity, $10^{2.5}$ from the increased occurrence frequency, and 10^1 from the increased proton flux compared to X-ray flux. As the contemporary proton fluence at 1 A.U. from the flare site averaged over a solar cycle is measured to be $f_p \simeq 200$ protons cm^{-2} s^{-1} with energies $E > 10$ MeV (Reedy 1996, see Appendix), the inferred proton fluence at 1 A.U. for solar-mass stellar systems during their first million years is $f_p \sim 10^7$ protons cm^{-2} s^{-1}. Note that, as the duration of a single powerful solar proton event is typically several hours and flares with $\log L_x(peak) > 28$ erg s^{-1} (below our detection limit) probably occurred several times a day, it is likely that the pre-main sequence Sun was producing high fluences of relativistic protons nearly continuously from overlapping magnetic flare events.

---

[4]A final multiplicative factor associated with the proton contribution of flares fainter than the $\log L_x \simeq$ 29.0 erg s^{-1} flare sensitivity limit of the Chandra observations can be included. But this may be relatively small because the frequency distribution of solar proton events is heavily weighted towards the strongest flares so the weaker flares, though more numerous, contribute relatively little to the total particle fluence.

It is useful for some theoretical calculations to estimate the luminosity of energetic protons rather than the fluence at 1 A.U. The conversion is not simple as proton ejection and propagation is guided by the magnetic fields and is not isotropic. If we roughly assume protons are ejected in an outward-facing hemisphere and that their average energy is $E_{20} = 20$ MeV, then the luminosity of $E > 10$ MeV protons inferred from the ONC flaring is $L_p \sim 2\pi d^2 f_p E_{20} = 5 \times 10^{29}$ $(d/1\text{A.U.})^2$ erg s^{-1}. The ratio L_p/L_x we infer for pre-main sequence flares is of order 10^{-1}, consistent with available knowledge of the energetics of powerful solar flares.

We also note that the directly observed value $< \log L_x > \simeq 30.3$ erg s^{-1} should be useful for computations of X-ray ionization and astrochemistry of the solar nebula and other circumstellar material around solar-mass pre-main sequence stars (e.g. Igea & Glassgold 1999; Aikawa & Herbst 1999; Glassgold, Feigelson, & Montmerle 2000; Glassgold et al. 2001).

6. From Orion X-ray flares to meteoritic isotopic anomalies

In this section, we discuss in some detail the degree of confidence in the line of reasoning linking the observations of ONC X-ray flares and the measurements of short-lived isotopic abundance anomalies in carbonaceous chondrites. We find that some links in the logical chain are strong while others suffer considerable uncertainty.

6.1. Do Orion results apply to the early Sun?

Our results show that the great majority of stars in our sample exhibit very high flaring levels during their first Myr. A critical element of our study's design is the completeness of the sample of pre-main sequence solar mass stars within well-defined observational criteria. The only selection bias within the ONC is the preference for unobscured stars in the evacuated region of the Messier 42 HII region over obscured stars lying in the undisturbed molecular cloud behind the HII region. We have not thought of any mechanism whereby this bias can affect magnetic activity.

While the X-ray luminosities of young stars have dependencies on mass and age which we have accounted for, there is no known dependence on their star forming environments. Although quantitative studies are lacking due to insufficiency of optical characterizations, *Chandra* studies of T Tauri stars in environments as sparse as the L1551 cloud in Taurus-Auriga (Bally et al., in preparation) and NGC 1333 region in Perseus (Getman et al. 2002) and as rich as the Rosette OB association (Townsley et al., in preparation) have similar X-ray

luminosity ranges, plasma temperatures and variability properties. With ~ 2000 stars, the ONC is roughly midway in log-mass between the richest star clusters and the sparse groups forming in low mass nearby molecular clouds. When equal logarithmic intervals of mass are considered, a given star has roughly equal probability of having formed in large and small clusters (Elmegreen & Efremov 1997). The flaring activity of ONC solar-mass stars can thus be applied to any solar mass star with considerable confidence.

The universality of enhanced flaring stands in contrast to competing models for external seeding of radioactive isotopes which require special conditions. For example, seeding by the passage of an AGB star during its dredge-up phases when freshly synthesized atoms will permeate its atmosphere (Wasserburg et al. 1994; Busso, Gallino, & Wasserburg 1999) is likely to apply in only $1 : 10^6$ star forming sites (Kastner & Myers 1994).

6.2. Do X-ray flares produce energetic protons?

In solar flares, the magnetic reconnection processes that heat plasma to X-ray temperatures can also accelerate and release charged particles with MeV energies (see Appendix). Particle acceleration is evidenced by variable nonthermal and circularly polarized radio continuum emission, gamma-ray emission lines from spallogenic nuclear excitation, and sudden enhancements of energetic particles propagating through the interplanetary medium. The processes are complex and not fully understood. The heating of plasma to X-ray temperatures and the acceleration of particles to MeV energies are sometimes nearly simultaneous and cospatial, but are often decoupled. For example, a multiwavelength study of the magnetically active T Tauri star V773 Tau showed several-fold decay of a radio flare simultaneous with a constant high level of X-ray emission over several hours (Feigelson et al. 1994). In the Sun, radio bursts associated with flares can occur on timescales of one second to many hours and span ≥ 4 orders of magnitude in frequency (Bastian, Benz, & Gary 1998). Only during the brief impulsive phases of some flares are radio, gamma-ray and hard X-ray emission nearly simultaneous and clearly originate from the same reconnection event.

However, despite the complexity of solar flare physics and the lack of a simple relationship between X-ray flares and solar energetic particles, the link is statistically strong. The NOAA Space Environment Center uses the integrated solar luminosity above 1×10^{26} erg s^{-1} (M5 level) in the $1.5 - 12$ keV band from the $GOES$ X-Ray Sensor to forecast the proton fluence that arrives at 1 A.U. hours to days later (Bornmann et al. 1996).

A strong statistical link also exists between X-ray emission and radio gyrosynchrotron from energetic electrons in the solar-stellar arena. The relationship $\log L_x \simeq 19.0 + 0.73 \log L_r$,

where L_r is expressed in erg s^{-1} Hz^{-1}, is found over 10 orders of magnitude in L_r, extending from solar microflares to the most magnetically active late-type stars (Benz & Guedel 1994). Radio gyrosynchrotron emission has been detected including several dozen weak-lined T Tauri stars at levels around 10^{25} erg s^{-1} Hz^{-1} at centimeter wavelengths, and in a few cases high fractions of circular polarization conclusively demonstrate that the emission is gyrosynchrotron from trans-relativistic electrons accelerated in strong magnetic fields (see reviews by André 1996; Feigelson & Montmerle 1999). Gyrosynchrotron emission is generally undetected from the earlier evolutionary phases, probably due to free-free absorption by ionized material associated with accretion and outflows. But variable circular polarized emission has been seen in three protostars, two of which also show X-ray flares (Phillips, Lonsdale, & Feigelson 1993; Feigelson, Carkner, & Wilking 1998; Getman et al. 2002). Young stars with the most powerful flares, including weak-lined T Tauri stars, generally show radio emission $1-2$ orders of magnitude above the level predicted by the Benz-Güdel relation. This is attributed to saturation of X-ray flares but not radio flares near the stellar surface (Güdel, Guinan, & Skinner 1997).

As it is difficult to imagine a magnetic reconnection process that accelerates electrons but not protons, these radio findings provide strong evidence that MeV protons are copiously produced in pre-main sequence flares.

6.3. Do the protons hit the disk?

There is considerable uncertainty about the spatial relationships between disk solids and energetic flare particles in young stellar system. While a vast literature attests to the presence of powerful and frequent magnetic flares in T Tauri stars, the geometry of the reconnecting fields is still under debate (Feigelson & Montmerle 1999). We consider three alternative geometries, each with a different implication for the efficiency of proton irradiation of disk material.

6.3.1. Stellar surface fields

Optical photometry and Doppler imaging of active regions, and Zeeman splitting of photospheric absorption lines demonstrate that T Tauri stars have multipolar magnetic fields like the Sun but greatly enhanced in strength and surface coverage. The Zeeman measurements indicate average surface field strengths $Bf \simeq 2-4$ G, where f is the surface fraction covered with fields (Valenti 2001). Study of X-ray flare emission during eclipses of

the magnetically active binary Algol show that its emission is confined to the close vicinity of the stellar surface (Schmitt & Favata 1999), but no similar direct measurement is available for T Tauri stars. Models of young stellar flare decays based on radiative cooling of an instantaneously heated plasma suggest magnetic loops much larger than the stellar radius. But models invoking continuous reheating are consistent with smaller loops of order $\simeq 0.1$ $R_\star$ in extent (Favata, Micela, & Reale 2001).

If the X-rays are produced from reconnecting multipolar fields near the stellar surface as in the Sun then, assuming a direct ballistic trajectory, 13% of the emission will impact a hypothetically flat thin disk at an oblique angle (Hartmann 1998, 98ff). Theoretical considerations (Chiang & Goldreich 1997) and direct imaging of protostellar disks (Bell et al. 1997) indicate disk flaring (i.e. vertical scale height increases with distance from the young star) is common on > 1 A.U. scales, so the impact fraction is likely higher. However, energetic protons released by reconnecting fields must follow magnetic field lines which are likely to have a complicated geometry that may differ substantially from the solar field. Some protons may be released into a closed dipole magnetosphere, while others may follow open lines that perpendicular to the disk that confine the bipolar outflows (Shu et al. 2000). It is unclear whether a substantial fraction of energetic protons would be focused onto the disk. This question may be answered by the next generation of radio interferometers which could image the spatial distribution of flare-generated MeV electrons (§6.3.4).

Two features in our *Chandra* Orion results suggest that pre-main sequence flares arise near the stellar surface as in main sequence stellar flares. First, short-duration secondary flares are seen superposed on the long decay phase of a powerful flare in a number of cases (see JW 470, 567 and 826 in Figure 3). This is commonly seen in powerful solar long duration flares as different portions of a complex active region release magnetic energy. Second, some of the ACIS spectra show emission lines indicative of elemental abundance anomalies seen in stars whose emission processes are definitely unrelated to circumstellar disks. A considerable number of ONC ACIS sources, including some solar analogs, show spectra suggesting overabundance of neon and underabundance of iron. This combination of plasma abundance anomalies, nicknamed the 'anti-FIP Effect' (First Ionization Potential), has been seen in the X-ray spectra of flares of magnetically active main sequence and RS CVn giant stars (Brinkman et al. 2001; Güdel et al. 2001). The reasons for these plasma abundance anomalies are still uncertain but are thought to involve the evaporation of chemically fractionated regions of the stellar surface by flare energetic particles. It is unclear whether a similar fractionation could occur at the surface of a circumstellar disk.

6.3.2. Star-disk fields

Considerable evidence suggests that young stars have strong dipole magnetic fields which extend out to the corotation radius of the circumstellar disk (see reviews by Hartmann 1998; Feigelson & Montmerle 1999; Shu et al. 2000). Star-disk field lines simultaneously funnel accreting material onto the stellar surface (this gas is responsible for T Tauri broad optical emission lines that had been formerly attributed to a dense stellar wind), and likely transfer stellar angular momentum from the star to a bipolar outflow (see however Stassun et al. 1999).

In this case, it is reasonable that some magnetic field lines will extend from the disk to portions of the disk that are not in corotation with the star and will thereby suffer twisting and reconnection. This might occur if the disk has inhomogeneous accretion rate (Shu et al. 1997), if the stellar rotation is not yet decelerated (Montmerle et al. 2000), or if field lines are coupled to the shearing layers in the Keplerian disk (Birk et al. 2000). Numerical MHD calculations indicate that the interaction between the stellar dipolar and disk toroidal fields is unstable and can erupt with a violent magnetic reconnection (Hayashi, Shibata, & Matsumoto 1996). In this geometry, the flare X-rays and particles are produced close to and above the inner disk, and spallation of inner disk material is likely to occur in an efficient manner. This is the geometry assumed in the meteoritic spallation calculations of Lee et al. (1998) and Gounelle et al. (2001) and in the chondrule melting model of Shu et al. (2001).

6.3.3. Disk fields

It is likely protostellar disks amplify embedded magnetic fields through turbulence and dynamo processes, and it is possible that violent reconnection occurs when these fields emerge at the disk surfaces. Ionization from cosmic rays and young stellar X-rays are sufficient to couple the largely neutral disk gas to field lines and induce turbulence via the magneto-rotational (Balbus-Hawley) instability over the outer layers of the protostellar disk (Gammie 1996; Igea & Glassgold 1999). Numerical MHD models show heating and ionization of a disk corona (Miller & Stone 2000), but these calculations do not include the physics for reconnection and flares. Detailed modeling of flaring from magnetic fields subject to the Keplerian shear of an accretion disk is just beginning (Romanova et al. 1998; Poutanen & Fabian 1999).

Disk magnetic fields and flares have also emerged in meteoritical studies. The 'remanent magnetism' of chondrules in a wide range of stony meteorites gives direct evidence for ~ 1 G fields in the solar nebula (Levy 1978). In addition, some models of chondrules melting

and proton spallation are based on irradiation from disk field flares: Levy & Araki (1989) consider flares in a disk corona during the earliest evolutionary phases, while Cameron (1995) considers flares at the interface between the young solar wind and a receding disk during a later pre-main sequence phase. In both cases, the advantage of disk flares is to produce chondrules and radioactive isotopes *in situ* at the Asteroid Belt where the parent bodies of meteorites are now found.

6.3.4. *Observational tests of magnetic geometry*

Two observational tests of these alternatives are feasible. First, some X-ray flares from young stars are sufficiently hot ($kT \geq 5$ keV) and luminous that the continuum around the Kα transitions of iron is seen with high signal-to-noise. Such cases provide the opportunity to see a fluorescent emission line reflected from neutral iron atoms in the circumstellar disk. This fluorescent line at 6.4 keV can be distinguished from the $6.6 - 6.9$ keV thermal line complex produced by the highly ionized iron species in the flare plasma at CCD spectral resolution. Double emission line complexes attributable to hot and cold iron have been reported in two very young protostellar systems: infrared source R1 in the Corona Australis Coronet Cluster using the ASCA SIS detector (Koyama et al. 1996) and YLW 16A in the ρ Ophiuchi cloud core using the Chandra ACIS-I detector (Imanishi, Koyama, & Tsuboi 2001). In both cases, the equivalent width of the two iron lines were comparable, indicating that the disk subtends a large solid angle when viewed by the X-ray emitting magnetic structure.

This is evidence against reconnection of magnetic fields very close to the stellar surface (§6.3.1), and favors a geometry where the reconnection occurs above the disk in a 'lamppost' configuration (§6.3.2-6.3.3). Fluorescent iron line emission under a variety of geometries has been investigated in the context of Seyfert galaxies and X-ray binary systems (Nayakshin & Kallman 2001, and references therein), although similar study has not yet been conducted specifically for protostellar systems. As in Seyferts, the high amplitude variability of the flare emission should be reproduced in the fluorescent line with time delays associated with the relative geometry of the emitting and reflecting components and the line-of-sight. This is a potentially powerful tool for understanding protostellar systems, but the limited signal-to-noise around 6.4 keV provided by existing telescopes permits only limited reverberation mapping. Imanishi, Koyama, & Tsuboi (2001) report that the emitting and reflecting components in YLW 16A vary together with a delay $< 10^4$ light-seconds indicating that the flare-disk distance is < 15 A.U. Higher signal-to-noise reverberation mapping studies may be very fruitful with planned high-throughput X-ray missions such as Constellation-X and XEUS.

The second method for measuring magnetic geometries in young stellar systems uses radio band Very Long Baseline Interferometry (VLBI) which can image the distribution of transrelativistic electrons emitting gyrosynchrotron radiation. It is likely that the spatial distribution of MeV protons is similar to that of MeV electrons, as both must follow the magnetic field lines from the sites of particle acceleration. A VLBI survey of several radio- and X-ray-bright young stellar objects in nearby star forming regions revealed extended emission on scales of ~ 1 mas or ~ 200 A.U. (Phillips, Lonsdale, & Feigelson 1991), but in at least one case the emission was found to arise from both components of a close binary (Phillips et al. 1996). There is one example of a clearly resolved nonthermal young stellar radio source: T Tau South, the embedded companion to the optically bright prototype T Tau, exhibits variable radio emission concentrated in two jets where each jet produces gyrosynchrotron with oppositely oriented circular polarization (Ray et al. 1997). If this geometry is ubiquitous, we might conclude that energetic protons produced by protostellar flares are transported away from the outer disk by the bipolar outflows. But it is still possible in this situation that the particles impact inner disk solids at the base of the outflow, as in the proton irradiation model of Shu et al. (1997) and Gounelle et al. (2001). The planned Extended Very Large Array and Atacama Large Millimeter Array should have the sufficient capabilities to resolve the magnetic structures containing relativistic particles in nearby YSOs. This requires mapping circularly polarized sub-milliJansky continuum emission on milliarcsecond scales.

6.4. Can the impacting protons produce the anomalies?

A full analysis of the spallogenic effect of the energetic protons in pre-main sequence stellar systems lies beyond the scope of this paper. We restrict our discussion to the relationship between two recent theoretical investigations of spallation in the solar nebula and the proton fluences inferred to be present in the present study.

Lee et al. (1998) and Gounelle et al. (2001) consider the effect of a powerful reconnection event occurring above the corotation radius of the circumstellar disk having $\log L_x = 5 \times 10^{30}$ erg s^{-1} and a luminosity in $E > 10$ MeV protons of $L_p = 4.5 \times 10^{29}$ erg s^{-1}. Their spallation model is applied to proto-CAI material near the disk corotation radius and produces observed abundances of several short-lived nuclides: ^{10}Be, ^{26}Al, ^{41}Ca, ^{53}Mn and ^{138}La but not ^{60}Fe. They treat self-shielding in CAIs ≥ 1 mm in size, which is important to reduce overproduction of ^{41}Ca. Their model requires specification of flaring magnetic field geometry (a 'lamppost'

loop over the inner disk), ^{3}He enrichment of flare particles[5], and a mechanism for dispersing the CAIs from the inner to the mid-disk region by temporary entrainment into the bipolar outflow.

Goswami, Marhas, & Sahijpal (2001) study the spallogenic production of ^{26}Al, ^{36}Cl, ^{41}Ca and ^{53}Mn by solar enegetic particles in the mid-disk region. They consider reactions on both gas- and solid-phase atoms using energetic protons and ^{4}He (but not ^{3}He) with self-shielding in the larger particles. The cause and geometry of the flare event is not specified. Proton fluxes are normalized to a time-averaged level of $f_p(E > 10 \text{ MeV}) \simeq 100$ protons cm^{-2} s^{-1} observed at 1 A.U. from the contemporary Sun. They find that meteoritic abundances of ^{41}Ca, ^{36}Cl and ^{53}Mn require 5×10^3 to 10^4-fold enhancement of the proton flux for 5×10^5 to several million years, while production of ^{26}Al requires enhancement factor of almost 10^5.

We find that both of these calculations of a solar nebula origin of meteoritic short-lived nuclei are fully consistent with the flare proton levels we infer are present during the first million years of the solar system. The X-ray and proton luminosities assumed by Gounelle et al. (2001) to explain the observed abundances of several nuclides are nearly identical to the values we find from ONC solar analogs (§5). The proton enhancement factors and irradiation durations required by Goswami, Marhas, & Sahijpal (2001) similarly consistent with the 10^5 enhancement over ~ 1 My that we infer from the Chandra ONC results (§5). Recall that their enhancement factors apply to particle fluences observed at a distance of 1 A.U. from the proton acceleration site, so that lower enhancement factors would be needed if the flaring magnetic structures were closer to the irradiated disk material, as in §6.3.2-6.3.3. Our observational findings on ONC solar analogs and these calculations of meteoritic isotopic anomalies from spallation by locally produced particles are thus completely compatible completely compatible with each other, except for unfavorable magnetic field geometries.

7. Conclusions

This study addresses long-standing puzzles regarding the origin of high energy processes in the solar nebula, as evidenced by petrologic, isotopic and cosmic ray tracers in ancient

---

[5]The overabundance of neon seen in the X-ray spectra of powerful stellar flares (Brinkman et al. 2001; Güdel et al. 2001, , §6.3.1) and the association of neon with helium abundances in solar energetic particles (Dwyer et al. 2001) support this idea. If it is due to a chemical fractionization by first ionization potential, then helium and neon abundances should be correlated in flare plasmas which are the likely source of accelerated particles as helium and neon have the highest first ionization potentials of all elements. Recall that helium lines cannot be detected in the X-ray plasmas because it is fully ionized.

pristine meteorites. Based on the general knowledge of enhanced X-ray flaring in pre-main sequence stars available a decade ago, Feigelson, Giampapa, & Vrba (1991) concluded that X-ray and radio flare studies of T Tauri stars "have a clear contribution to these debates concerning meteoritic properties: *invoking high levels of energetic particle or radiation fluxes associated with magnetic activity in the early Sun is no longer ad hoc*". The *Chandra* measurements of flaring in Orion pre-main sequence solar analogs presented here confirm this statement and provide details that were not available earlier.

We have established that virtually all analogs of the ≤ 1 My old pre-main sequence Sun exhibited X-ray flares that are $10^{1.5}$ times more powerful and $10^{2.5}$ times more frequent than the most powerful flares seen on the contemporary Sun (§5). The inferred energetic proton flux is increased by an additional factor of 10^1 above the X-ray flux, although the physical mechanism underlying this enhancement factor is uncertain. We infer that the proton fluence in the early Sun is about 10^5 times the time-averaged levels produced by the contemporary Sun.

The line of reasoning linking the ONC X-ray measurements to solar nebular isotopic anomalies has several steps. The completeness of our sample and ubiquity of strong X-ray flaring during the first My (though a decline in activity appears in some stars during the $1-10$ My period, §4.1) argues strongly that the early Sun produced such flares (§6.1). There are also strong reasons, based on YSO radio gyrosynchrotron measurements and analogy with solar flare physics, to believe that the ONC X-ray flares are accompanied by high proton fluences (§6.2). The geometry of the reconnecting magnetic fields and consequence fraction of flare protons that impact the disk is uncertain, particularly at distant locations in the Asteroid Belt where meteorites parent bodies are now found (§6.3). However, the report of the 6.4 keV iron fluorescent line in protostellar spectra strongly suggests that the X-rays, and by reasonable inference the protons, efficiently impact the disk. Unless the flare geometries are unfavorable, we find the inferred proton flux on the disk is sufficient to produce the observed CAI abundances of several important short-lived radioactive isotopes (§6.4).

Our study thus strengthens the astronomical foundation for local proton spallation models of meteoritic isotopic anomalies. However, it cannot not establish the entire theory. For example, it is not clear that a local spallation model can account for meteoritic ^{60}Fe (Lee et al. 1998) or for the evidence that the abundance of ^{53}Mn was greater in the outer solar nebula than the inner nebula (Shukolyukov & Lugmair 2000). It seems plausible that *both* external seeding and internal spallation may have been sources of short-lived nuclides in the solar nebula. Meyer & Clayton (2000) also emphasize that several extinct radioactive isotopes in meteorites can be attributed to ongoing nucleosynthesis in the Galaxy.

Although our attention here has been principally directed towards the isotopic anoma-

lies, the findings here may similarly important implications for the other meteoritic characteristics demanding high energy processes. Our results clearly support the extensive evidence for a flare spallogenic origin of excess ^{21}Ne and particle tracks in gas-rich meteoritic silicate grains (e.g. Caffee et al. 1987; Woolum & Hohenberg 1993; Caffee & Nishiizumi 2001). The contribution of flare energetic particles to disk and outflow ionization might be added to existing calculations treating Galactic cosmic ray and stellar X-ray ionization (e.g. Gammie 1996; Igea & Glassgold 1999). The effects of flare radiation and shocks on disk solids, including the possibility of flash melting the chondrules, have been considered in detail in only limited contexts (Levy & Araki 1989; Shu et al. 2001). More extensive calculations of such effects based on various possible magnetic geometries may now be warranted.

A. Comparison with contemporary solar flares

The powerful X-ray flares we detect in ONC solar analogs closely resemble the X-ray emission from relatively rare powerful solar flares. Such flares constitute long duration events (10-20 hours) in the soft X-ray band and are associated with gradual hard burst events (GHXs) with hardening in the X-ray band from roughly 40 to 200 keV. These events are also associated with type II and IV bursts in the metric radio band, coronal mass ejections (CMEs), and prompt solar energetic particle events (SEPs) in measurements of the interplanetary medium. These properties have been nicknamed the Big Flare Syndrome (Kahler 1982) because small to moderate events often lack one or more of these features.

While their physics is very complex and still debated, successful models for many properties of solar eruptive events have been developed. Their power and duration require continuing release of energy previously stored in magnetic fields at the solar surface. In many models, a flux rope rises in an arcade of field loops, resulting in field reconnection to a simpler geometry and the ejection of magnetic flux at velocities of 1000-2000 km s^{-1} (Priest & Forbes 2000, §11.1). The outer loops of the arcade are filled with 10^7 K plasma, while the inner loops have 10^4 plasma appearing as two ribbons of Hα emission (hence the nomenclature 'two-ribbon flare'). Both radiative and conductive cooling may be important in the heated loops. Some gas flows downward onto the surface, evaporating chromospheric material which then flows upwards along other field lines; this may be responsible for unusual elemental abundances seen in some solar and stellar X-ray flare plasmas.

The production of energetic (MeV) particles is less well understood but may involve several processes acting alone or in consort: direct acceleration by strong electric fields between different magnetic regions of the flare, or acceleration in MHD waves, shocks, instabilities or turbulence (Miller et al. 1997; Priest & Forbes 2000, , §13). Particles can be accelerated both on small scales during the impulsive phase of a flare, on larger scales within the coronal mass ejection, or on very large scales in corotating interaction regions of the solar wind. During the brief impulsive flare, gamma-ray line and continuum emission, neutrons from nuclear collisions, microwave gyrosynchrotron, and hard X-ray bremsstrahlung can be present. Impulsive particle acceleration appears to be very efficient with $\sim 10^{31}$ erg produced in each of energetic electrons, protons and ions in an X-class flare. Protons can acquire up to GeV energies. However, many of these particles remain trapped in solar fields and are not ejected into the interplanetary medium.

During $1989 - 1997$ (solar cycle 22), a period of about 3000 days, the *Geosynchronous Operational Environmental Satellite (GOES) 7* satellite detected about 20 solar flares with $28.0 \leq \log L_x(peak) \leq 29.0$ erg s^{-1} in the $1.6 - 12$ keV ($1 - 8$ Å) band (Sammis, Tang, & Zirin 2000). The recurrence rate of these maximally X-ray luminous solar flares, which are

$\simeq 100$ times weaker than the typical ONC flare is about one flare per year (3×10^7 s).

Reedy (1996, updated in Reedy 2001) has obtained an understanding of the fluence of solar enegetic particles at 1 A.U. He combines direct spacecraft measurements of solar energetic particles from 1965-91 (solar cycles $20 - 22$) with indirect measurements from ^{14}C in tree ring data and abundances of spallogenic nuclides in lunar rocks. The results are all consistent with a constant time-averaged omnidirectional proton flux over the past $10^1 - 10^6$ yr of $f_p \simeq 200$ protons cm^{-2} s^{-1} at 1 A.U. for energies $E > 10$ MeV. Most of these protons are produced in the most powerful flares as the integrated frequency of events with fluence F is given by[6] $N(F > F_o) \simeq 1(F_o/10^9 \text{protons cm}^{-2})^{-0.4}$ yr^{-1} over the range $10^7 < F_o < 10^{10}$ protons cm^{-2}.

Reedy finds a steep cutoff in solar particle events with fluences above 10^{10} protons cm^{-2}. The reasons for this are unknown. We assume here that this limit applies only to contemporary solar flares, and that the proton fluences associated with young stellar flares exhibiting X-ray luminosities far above those seen in the Sun today can considerably exceed this solar limit.

It can be useful to examine the behavior of individual powerful solar flares as analogs for ONC flares. Consider, for example, a typical strong solar flare and proton event like the 23-24 March 1991 flare (SOLTIP Interval 1; Shea & Smart 1996, see details in Watanabe 1995). The $GOES - 7$ lightcurve shows the Sun's X-ray luminosity rise over $\simeq 4$ hours from 8×10^{24} to a peak of 1×10^{26} erg s^{-1} in the $1.6 - 12$ keV band. The X-ray decay over $\simeq 20$ hours is accompanied by several $\simeq 1$ hr secondary flares with peak luminosities comparable to the principal flare. The flare was followed by an increase in $E > 1$ MeV proton fluence from 10^1 to $10^{5.5}$ protons cm^{-2} s^{-1} ster^{-1} at 1 A.U. over the next day, which produced a major geomagnetic storm, terrestrial electromagnetic anomalies, and a prominent decrease in the Galactic cosmic ray intensity. Note, however, that the flare on the previous day, 22 March, which was an intense gamma-ray and relativistic neutron emitter, produced a brief impulsive X-ray spike but not a long duration soft X-ray event.

An exceptionally powerful group of solar flares occurred over two weeks in June 1991 (SOLTIP Interval 2). Several received the highest possible X-ray classification >X12. The 1 June 1991 flare, for example, produced: (a) $10^{32} - 2 \times 10^{33}$ erg in X-rays (the exact value is unknown due to saturation of the $GOES$ detectors); (b) more than $10^{32} - 10^{34}$ erg injected

---

[6]This relation differs somewhat from the differential distribution $dN/dE \propto E^{-1.15}$ reported by van Hollebeke, Ma Sung, & McDonald (1975). While indices ranging from -1.15 to -1.4 have been reported for the distribution of solar proton events, they are always substantially flatter than the -1.8 index found for the distribution of X-ray peak fluxes (Hudson 1991).

(but not necessarily released into the interplanetary medium) in > 20 keV electrons; (c) $\sim 10^{33}$ erg in MeV nucleons; (d) a powerful flux of neutrons; and (e) strong shocks in the interplanetary medium driven by flare-induced ^{3}He-enriched coronal mass ejection (Kane et al. 1995; Watanabe, T. 1995; Ramaty et al. 1997; Murphy et al. 1999; Clayton, Guzik, & Wefel 2000). The peak X-ray luminosity in the *GOES* $1.6 - 12$ keV band is estimated to be $\log L_x \simeq 10^{28.5}$ erg s^{-1}. No major proton flare was seen at the Earth from this event as the interplanetary magnetic field lines carrying the particles fortuitously missed the Earth.

REFERENCES

Adams, F. C. & Laughlin, G. 2001, Icarus, 150, 151

Aikawa, Y. & Herbst, E. 1999, A&A, 351, 233

André, P. 1996, in Radio Emission from the Stars and the Sun, ASP Conf. Ser. 93, 273

Arnould, M., Paulus, G., & Meynet, G. 1997, A&A, 321, 452

Babu, G. J. & Feigelson, E. D. 1996, Astrostatistics, London:Chapman and Hall

Bally, J. 2001, in Tetons 4: Galactic Structure, Stars and the Interstellar Medium, ASP Conf. Ser. 231, in press

Bastian, T. S., Benz, A. O., & Gary, D. E. 1998, ARA&A, 36, 131

Bell, K. R., Cassen, P. M., Klahr, H. H., & Henning, T. 1997, ApJ, 486, 372

Benz, A. O. & Guedel, M. 1994, A&A, 285, 621

Birk, G. T., Schwab, D., Wiechen, H., & Lesch, H. 2000, A&A, 358, 1027

Bloemen, H. et al. 1999, ApJ, 521, L137

Bornmann, P. L., Heckman, G., Hirman, J., Speich, D., Kunches, J., & Zwickl, R. 1996, in Solar Drivers of the Interplanetary and Terrestrial Disturbances, ASP Conf. Ser. 95, 137

Brinkman, A. C. et al. 2001, A&A, 365, L324

Busso, M., Gallino, R., & Wasserburg, G. J. 1999, ARA&A, 37, 239

Caffe, M. W., Hohenberg, C. M., Swindle, T. D., & Goswami, J. N. 1987, ApJ, 313, L31

Caffee, M. W. & Nishiizumi, K. 2001, Meteoritics and Planetary Science, 36, 429

Cameron, A. G. W. & Truran, J. W. 1977, Icarus, 30, 447

Cameron, A. G. W. 1995, Meteoritics, 30, 133

Cameron, A. G. W. 2001, ApJ, 562, 456

Chiang, E. I. & Goldreich, P. 1997, ApJ, 490, 368

Clayton, D. D., Dwek, E., & Woosley, S. E. 1977, ApJ, 214, 300

Clayton, D. D. 1994, Nature, 368, 222

Clayton, D. D. & Jin, L. 1995, ApJ, 451, L87

Clayton, E. G., Guzik, T. G., & Wefel, J. P. 2000, Sol. Phys., 195, 175

Crosby, N. B., Aschwanden, M. J., & Dennis, B. R. 1993, Sol. Phys., 143, 275

D'Antona, F. & Mazzitelli, I. 1997, Memorie della Societa Astronomica Italiana, 68, 807

de Geus, E. J. 1992, A&A, 262, 258

Dwyer, J. R., Mason, G. M., Mazur, J. E., Gold, R. E., Krimigis, S. M., Möbius, E., & Popecki, M. 2001, ApJ, 563, 403

Elmegreen, B. G. & Efremov, Y. N. 1997, ApJ, 480, 235

Favata, F., Micela, G., & Reale, F. 2001, A&A, 375, 485

Feigelson, E. D. 1982, Icarus, 51, 155

Feigelson, E. D. 1990, Errors, Bias and Uncertainties in Astronomy, Cambridge University Press, 213

Feigelson, E. D., Giampapa, M. S., & Vrba, F. J. 1991, in The Sun in Time, University Arizona Press, 658

Feigelson, E. D., Casanova, S., Montmerle, T., & Guibert, J. 1993, ApJ, 416, 623

Feigelson, E. D., Welty, A. D., Imhoff, C., Hall, J. C., Etzel, P. B., Phillips, R. B., & Lonsdale, C. J. 1994, ApJ, 432, 373

Feigelson, E. D., Carkner, L., & Wilking, B. A. 1998, ApJ, 494, L215

Feigelson, E. D. & Montmerle, T. 1999, ARA&A, 37, 363

Feigelson, E. D., Broos, P., Gaffney, J. A., Garmire, G. P. Hillenbrand, L. A., Pravdo, S. H., Townsley, L., & Tsuboi, Y. 2001, ApJ, submitted (F01)

Feigelson, E. D., Gaffney, J. A., Garmire, G. P. Hillenbrand, L. A., & Townsley, L., 2002, in preparation

Gammie, C. F. 1996, ApJ, 457, 355

Garmire, G., Feigelson, E. D., Broos, P., Hillenbrand, L. A., Pravdo, S. H., Townsley, L., & Tsuboi, Y. 2000, AJ, 120, 1426

Getman, K., Feigelson, E. D., Townsley, L., Bally, J., Lada, C. J. & Reipurth, B. 2002, in preparation

Glassgold, A. E., Feigelson, E. D., & Montmerle, T. 2000, Protostars and Planets IV, 429

Glassgold, A. E., Shang, H., Shu, F. H., & Lizano, S. 2001, BAAS, meeting 198, #28.02

Goswami, J. N. & Vanhala, H. A. T. 2000, in Protostars and Planets IV, University Arizona Press, 963

Goswami, J. N., Marhas, K. K., & Sahijpal, S. 2001, ApJ, 549, 1151 (Erratum: ApJ, 552, 912)

Gounelle, M., Shu, F. H., Shang, H., Glassgold, A. E., Rehm, K. E., & Lee, T. 2001, ApJ, 548, 1051

Güdel, M., Guinan, E. F., & Skinner, S. L. 1997, ApJ, 483, 947

Güdel, M., Audard, M., Sres, A., Wehrli, R., Behar, E., Mewe, R., Raassen, A. A. J. J. & Magee, H. 2001, in Stellar Coronae in the Chandra and XMM-Newton Era, ASP Conf. Ser., in press (astro-ph/0109265)

Hartmann, L. 1998, Accretion processes in star formation,Cambridge University Press

Hayashi, M. R., Shibata, K., & Matsumoto, R. 1996, ApJ, 468, L37

Herbst, W. 1989, AJ, 98, 2268

Hewins, R. H., Jones, R. H., & Scott, E. R. D. 1996, Chondrules and the Protoplanetary Disk, Cambridge University Press

Hillenbrand, L. A. 1997, AJ, 113, 1733

Hillenbrand, L. A. & Carpenter, J. M. 2000, ApJ, 540, 236

Hoyle, F., Fowler, W. & Greenstein, J. 1962, Geophys. J. Roy. Astr. Soc., 6, 148

Hudson, H. S. 1991, Sol. Phys., 133, 357

Igea, J. & Glassgold, A. E. 1999, ApJ, 518, 848

Imanishi, K., Koyama, K., & Tsuboi, Y. 2001, ApJ, 557, 747

Jones, B. F. & Walker, M. F. 1988, AJ, 95, 1755

Jones, R. H., Lee, T., Connolly, H. C., Love, S. G., & Shang, H. 2000, in Protostars and Planets IV, University Arizona Press, 927

Kahler, S. W. 1982, J. Geophys. Res., 87, 3439

Kane, S. R., Hurley, K., McTiernan, J. M., Sommer, M., Boer, M., & Niel, M. 1995, ApJ, 446, L47

Kastner, J. H. & Myers, P. C. 1994, ApJ, 421, 605

Kastner, J. H., Zuckerman, B., Weintraub, D. A., & Forveille, T. 1997, Science, 277, 67

Kastner, J. H., Huenemoerder, D. P., Schulz, N. S., Canizares, C. R. & Weintraub, D. A. , 2001 submitted, astro-ph/0111049

Koyama, K., Hamaguchi, K., Ueno, S., Kobayashi, N., & Feigelson, E. D. 1996, PASJ, 48, L87

Lamzin, S. A. 1999, Astronomy Letters, 25, 430

Lee, T. 1978, ApJ, 224, 217

Lee, T., Shu, F. H., Shang, H., Glassgold, A. E., & Rehm, K. E. 1998, ApJ, 506, 898

Levy, E. H. 1978, Nature, 276, 481

Levy, E. H. & Araki, S. 1989, Icarus, 81, 74

Mathieu, R. D. 1994, ARA&A, 32, 465

McKeegan, K. D., Chaussidon, M., Robert, F. 2000, Science, 289, 1334

Meyer, B. S. & Clayton, D. D. 2000, Space Science Reviews, 92, 133

Miller, J. A. et al. 1997, J. Geophys. Res., 102, 114631

Miller, K. A. & Stone, J. M. 2000, ApJ, 534, 398

Montmerle, T., Grosso, N., Tsuboi, Y., & Koyama, K. 2000, ApJ, 532, 1097

Murphy, R. J., Share, G. H., Delsignore, K. W., & Hua, X.-M. 1999, ApJ, 510, 1011

Nayakshin, S. & Kallman, T. R. 2001, ApJ, 546, 406

Neuhäuser, R., Sterzik, M. F., Schmitt, J. H. M. M., Wichmann, R., & Krautter, J. 1995, A&A, 297, 391

O'dell, C. R. 2001, ARA&A, 39, 99

Okazaki, R., Takaoka, N., Nagao, K., Sekiya, M., & Nakamura, T. 2001, Nature, 412, 795

Peres, G., Orlando, S., Reale, F., Rosner, R., & Hudson, H. 2000, ApJ, 528, 537

Phillips, R. B., Lonsdale, C. J., & Feigelson, E. D. 1991, ApJ, 382, 261

Phillips, R. B., Lonsdale, C. J., & Feigelson, E. D. 1993, ApJ, 403, L43

Phillips, R. B., Lonsdale, C. J., Feigelson, E. D., & Deeney, B. D. 1996, AJ, 111, 918

Poutanen, J. & Fabian, A. C. 1999, MNRAS, 306, L31

Priest, E. & Forbes, T. 2000, Magnetic reconnection: MHD theory and applications, Cambridge University Press

Ramaty, R., Mandzhavidze, N., Barat, C., & Trottet, G. 1997, ApJ, 479, 458

Rao, M. N., Garrison, D. H., Palma, R. L., & Bogard, D. D. 1997, Meteoritics & Plan. Sci., 32, 531

Ray, T. P., Muxlow, T. W. B., Axon, D. J., Brown, A., Corcoran, D., Dyson, J., & Mundt, R. 1997, Nature, 385, 415

Reedy, R. C. 1996, in Solar Drivers of the Interplanetary and Terrestrial Disturbances, ASP Conf. Ser. 95, 429

Reedy, R. C. 2001, Meteoritics & Plan. Sci., 36, A172

Rice, J. B. & Strassmeier, K. G. 1996, A&A, 316, 164

Romanova, M. M., Ustyugova, G. V., Koldoba, A. V., Chechetkin, V. M., & Lovelace, R. V. E. 1998, ApJ, 500, 703

Sammis, I., Tang, F., & Zirin, H. 2000, ApJ, 540, 583

Schmitt, J. H. M. M. & Favata, F. 1999, Nature, 401, 44

Schulz, N. S., Canizares, C., Huenemoerder, D., Kastner, J. H., Taylor, S. C., & Bergstrom, E. J. 2001, ApJ, 549, 441

Shea, M. A. & Smart, D. F. 1996, in Solar Drivers of the Interplanetary and Terrestrial Disturbances, ASP Conf. Ser. 95, 266

Shukolyukov, A. & Lugmair, G. ;. W. 2000, Space Science Reviews, 92, 225

Shu, F. H., Shang, H., Glassgold, A. E., & Lee, T. 1997, Science, 277, 1475

Shu, F. H., Najita, J. R., Shang, H., & Li, Z.-Y. 2000, in Protostars and Planets IV, University Arizona Press, 789

Shu, F. H., Shang, H., Gounelle, M., Glassgold, A. E., & Lee, T. 2001, ApJ, 548, 1029

Stahler, S. W. 1983, ApJ, 274, 822

Stassun, K. G., Mathieu, R. D., Mazeh, T., & Vrba, F. J. 1999, AJ, 117, 2941

Stelzer, B. & Neuhäuser, R. 2001, A&A, 377, 538

Strassmeier, K. G. & Rice, J. B. 1998, A&A, 330, 685

Taylor, S. R. 1992, Solar System Evolution, Cambridge University Press

Valenti, J. 2001, in Magnetic Fields Across the Hertzsprung-Russell Diagram, ASP Conf. Ser. 248, in press

van Hollebeke, M. A. I., Ma Sung, L. S., & McDonald, F. B. 1975, Sol. Phys., 41, 189

Walter, F. M. & Barry, D. C. 1991, in The Sun in Time, University Arozona Press, 633

Wasserburg, G. J., Busso, M., Gallino, R., & Raiteri, C. M. 1994, ApJ, 424, 412

Watanabe, T. (ed.), Proc. Second SOLTIP Symposium, Mito, Japan:Ibaraki Univ

Weisskopf, M. C., O'Dell, S. L. & van Speybroeck, L. P., 1996, Proc. SPIE, 2805, 2

Woolum, D. S. & Hohenberg, C. 1993, in Protostars and Planets III, University Arizona Press, 903

Wuchterl, G. & Klessen, R. S. 2001, ApJ, 560, L185

Table 1.   X-ray properties of pre-main sequence solar analogs in the ONC

| ACIS source | | Optical properties | | | | | X-ray properties | | | | | | | | |
Src #	CXOONC J	JW	$\log L_*$ $(L_\odot)$	A_V (mag)	$\log t$ (yr)	Disk	C_{xtr}	CR_1 (cts ks^{-1})	CR_2	Var cl	$\log N_H$ (cm^{-2})	kT (keV)	S.F.	$\log L_x$ (erg s^{-1})	$\log L_x/L_*$
$\cdots$	$\cdots$	62	0.4	5.3	6.2	$-$	<30	$\cdots$	$\cdots$	$\cdots$	$\cdots$	$\cdots$	$\cdots$	<29.5	<-4.5
43	053451.5-052512	123	0.3	3.1	6.4	$+$	436	4.8	5.9	Const	21.4	1.4	$\star$	29.8	-4.1
109	053500.4-052513	198	-0.4	0.6	6.6	$+$	586	8.5	5.6	Pos fl	21.3	3.2	$\cdots$	30.1	-3.1
179	053505.7-052418	278	-0.1	1.7	6.2	$+$	63	0.4	1.2	LT Var	21.5	4.2	$\cdots$	29.2	-4.3
185	053506.2-052202	286	0.0	3.9	6.1	$+$	1182	15.8	13.7	Const	22.1	2.0	$\star$	30.5	-3.1
218	053508.3-052829	320	-0.1	3.6	6.9	$+$	40	0.6	0.2	Pos fl	22.4	2.3	$\star$	29.1	-4.4
229	053508.8-053149	328	0.1	1.2	6.1	$+$	277	$\cdots$	7.6	Flare	20.9	4.5	$\cdots$	30.4	-3.3
230	053508.9-052959	330	0.5	0.9	5.9	$-$	1724	27.9	10.7	Flare	$\cdots$	0.8/2	$\star$	30.5	-3.6
253	053510.2-052321	341	-0.8	0.0	7.5	$\cdots$	754	9.1	9.9	Pos fl	22.1	2.2	$\star$	30.3	-2.5
284	053511.4-052602	365	0.9	2.3	5.5	$+$	2873	51.4	13.8	Pos fl	21.4	1.9	$\cdots$	30.8	-3.7
302	053511.9-051926	370	0.7	5.5	5.6	$+$	445	5.0	6.7	Const	21.8	2.6	$\cdots$	30.0	-4.3
307	053511.9-052033	373	1.0	5.9	<5.5	$+$	1378	15.1	19.8	Pos fl	21.9	2.0	$\cdots$	30.5	-4.1
443	053514.9-052239	454	0.8	2.4	<5.5	$+$	2095	13.3	41.2	Flare	21.5	2.3	$\star$	30.7	-3.7
448	053514.9-052159	457	0.5	2.1	5.6	$+$	1735	17.2	26.6	Flare	21.5	2.0	$\cdots$	30.5	-3.6
457	053515.1-052254	463	0.8	2.7	<5.5	$\cdots$	193	1.8	3.6	Pos fl	21.6	5.5	$\cdots$	29.7	-4.7
468	053515.3-052215	470	0.9	3.8	<5.5	$+$	1230	21.8	8.6	Flare	22.0	3.6	$\cdots$	30.6	-3.9
501	053515.8-052322	488a	0.1	0.0	6.7	$+$	184	1.8	2.9	Const	<20.0	>10	$\star$	29.5	-4.2
520	053516.0-052036	504b	0.2	2.7	6.0	$\cdots$	1020	16.9	7.2	Pos fl	21.4	2.0	$\cdots$	30.2	-3.6
582	053517.2-052131	544	1.3	2.9	<5.5	$-$	1909	15.2	34.6	Flare	21.5	2.4	$\cdots$	30.6	-4.3
590	053517.3-052400	549	0.4	6.2	5.7	$+$	56	0.6	0.8	Const	22.1	2.4	$\star$	29.4	-4.6
602	053517.5-052256	553a	0.9	3.6	<5.5	$\cdots$	456	3.4	8.1	LT Var	21.6	3.3	$\cdots$	29.4	-5.1
604	053517.5-051740	550	1.1	8.1	<5.5	$+$	3636	50.4	37.0	Posfl	$\cdots$	1/2.4	$\cdots$	31.1	-3.6
626	053517.9-052245	567	1.5	1.5	<5.5	$-$	9016	24.0	212.5	Flare	21.5	5.8	$\cdots$	31.7	-3.4
662	053518.6-052313	596	0.7	3.8	5.7	$+$	2274	45.6	3.9	Flare	$\cdots$	0.1/4	$\cdots$	30.9	-3.4
664	053518.7-052256	598a	0.8	4.2	5.6	$\cdots$	456	3.5	8.4	Pos fl	22.0	2.1	$\cdots$	30.1	-4.3
675	053518.9-052052	605	-0.8	1.3	7.2	$+$	242	2.2	4.0	Pos fl	21.9	2.6	$\cdots$	29.9	-2.9
676	053518.9-051613	601	0.1	0.5	6.4	$-$	993	13.3	10.7	Flare	<20.0	1.1	$\star$	30.1	-3.6
682	053519.0-052349	607	0.1	2.5	6.8	$+$	28	0.4	0.2	Const	<20.0	>10	$\cdots$	28.8	-4.9
751	053520.8-052121	662	-0.5	1.0	6.9	$+$	17	0.2	0.2	Const	22.2	1.0	$\cdots$	28.5	-4.6
790	053521.8-052354	698	0.5	1.0	5.9	$+$	202	4.6	2.4	Flare	21.6	2.2	$\cdots$	29.6	-4.5
805	053522.1-052424	707	0.7	2.3	5.8	$\cdots$	609	7.4	7.8	Pos fl	21.8	2.1	$\cdots$	30.1	-4.2
808	053522.3-052029	706	0.4	0.7	6.0	$-$	652	9.6	6.0	LT Var	<20.0	1.0	$\star$	29.9	-4.1
814	053522.4-052201	712	0.3	4.0	6.1	$+$	531	7.6	5.5	Pos fl	21.8	2.5	$\cdots$	30.1	-3.8
848	053523.6-052332	738	-0.2	1.5	6.4	$\cdots$	2906	56.0	14.1	Flare	21.9	2.8	$\cdots$	30.9	-2.5
889	053525.0-052258	766a	0.6	4.4	5.9	$\cdots$	524	5.1	8.3	Pos fl	21.8	2.2	$\star$	30.1	-4.1

Table 1—Continued

| ACIS source		Optical properties					X-ray properties								
Src #	CXOONC J	JW	$\log L_*$ $(L_\odot)$	A_V (mag)	$\log t$ (yr)	Disk	C_{xtr}	CR_1 (cts	CR_2 ks^{-1})	Var cl	$\log N_H$ (cm^{-2})	kT (keV)	S.F.	$\log L_x$ (erg s^{-1})	$\log L_x/L_*$
890	053525.0-052346	769	0.5	1.9	5.5	−	719	10.7	6.7	Flare	21.1	1.5	⋆	30.0	-4.1
929	053527.3-052336	810	0.5	3.9	5.6	+	1127	7.0	22.7	Flare	21.6	2.6	⋯	30.4	-3.7
949	053528.2-052458	826	-0.6	0.0	6.8	+	2586	8.3	61.3	Flare	21.9	2.6	⋆	30.8	-2.2
969	053529.9-053252	847	0.8	0.5	5.6	−	608	⋯	17.0	Pos fl	21.0	1.6	⋯	30.6	-3.8
990	053531.2-052340	868	0.2	2.1	6.0	+	159	1.1	1.0	Const	21.4	2.7	⋯	29.5	-4.3
1022	053534.9-052914	907	0.2	1.4	6.3	−	1138	9.8	17.4	LT Var	<20.0	1.1	⋆	30.2	-3.6
1025	053535.3-052127	911	0.2	1.2	6.0	+	940	11.7	10.1	LT Var	21.0	1.3	⋆	30.1	-3.7
⋯	⋯	991	0.0		6.8	−	<50	⋯	⋯	⋯	⋯	⋯	⋯	<29.6	<-4.0
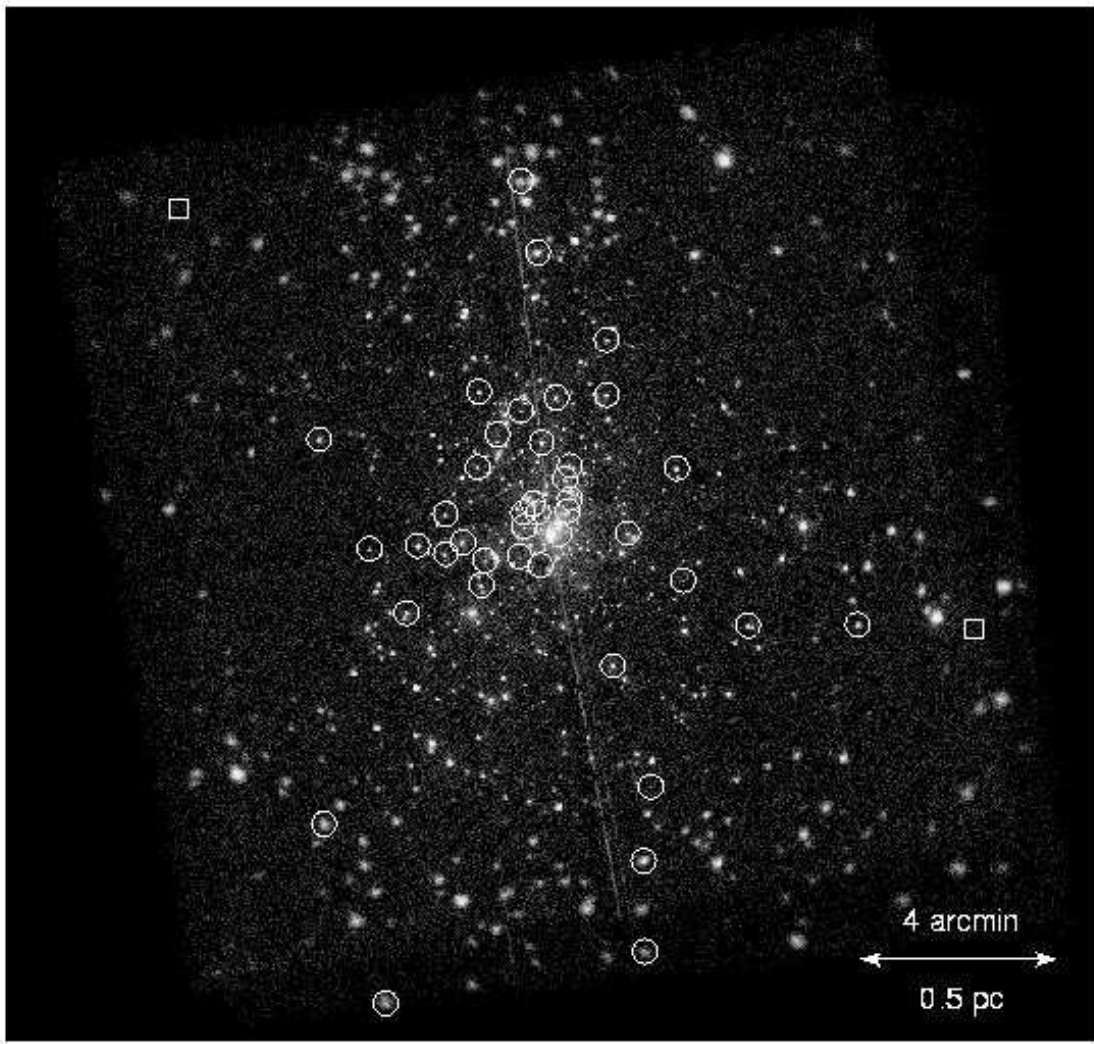
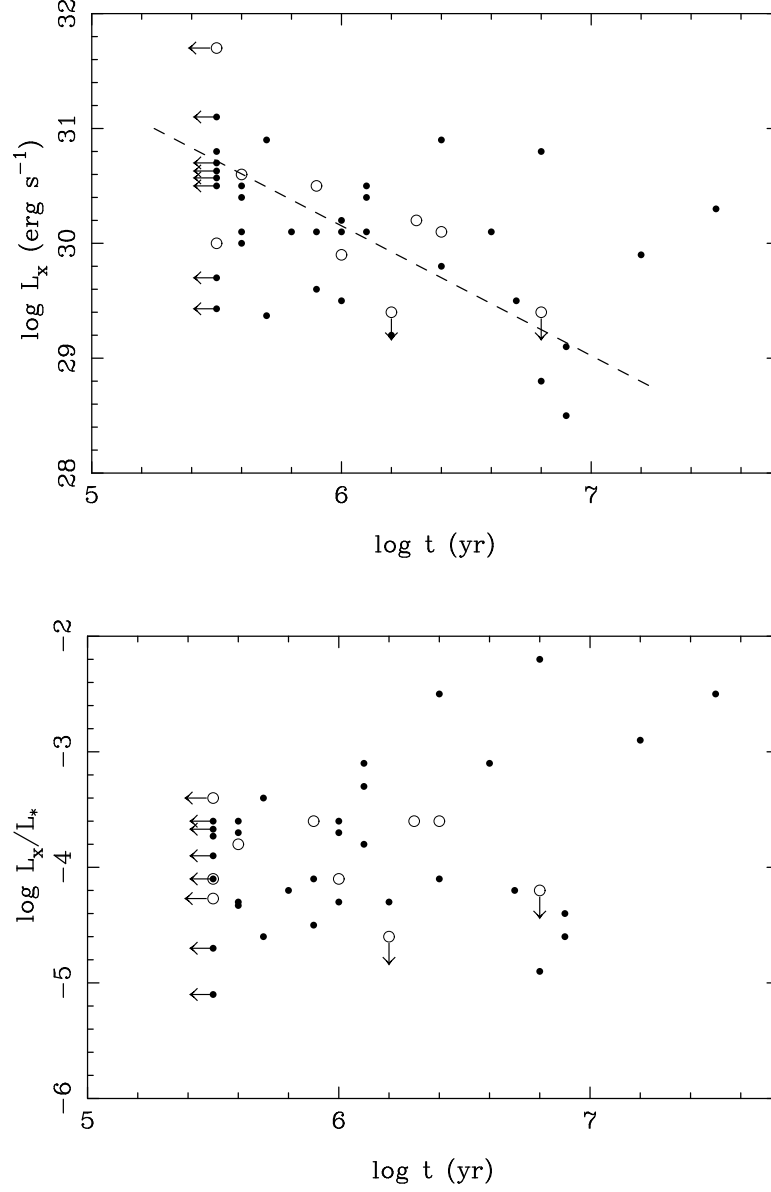Fig. 1.— The Chandra ACIS-I image of the Orion Nebula Cluster with 43 $0.7 < M < 1.4$

Fig. 2.— (a) Plot of the time-averaged X-ray luminosity in the $0.5 - 8$ keV band against the estimated stellar age for ONC solar analogs. (b) Plot of the ratio between X-ray and bolometric luminosities against age. Filled circles represent stars with evidence for circumstellar disks (or with no information on disks), and open circles represent stars without disks.
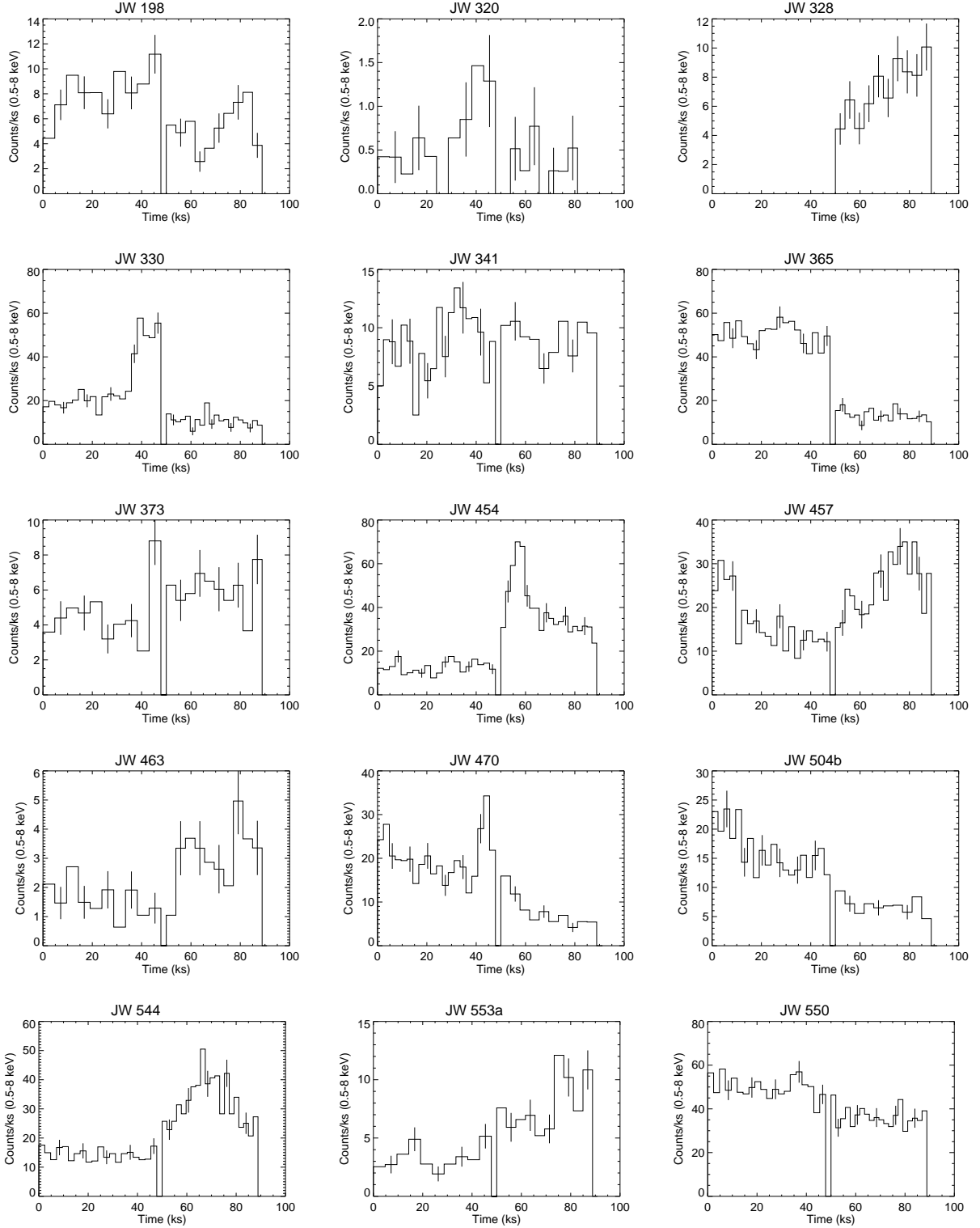
Fig. 3.— X-ray lightcurves of solar analog stars in the Orion Nebula Cluster exhibiting intraday variability (Variability Class 'Possible flare' and 'Flare'). For convenience, the two observations obtained on 12 Oct 1999 and 1 Apr 2000 are concatenated such that the second observation starts at Time = 50 ks. JW 328 and JW 847 were outside the field of view during one observation. Binwidths are set in each panel to give about 20 counts per bin; typical $\sqrt{N}$ uncertainties are shown.